



# Thermogravimetric analysis and kinetics characteristics of typical grains

Congxue Yao<sup>1</sup> · Xin Wang<sup>1</sup> · Yifan Zhou<sup>1</sup> · Xin Jin<sup>1</sup> · Lei Song<sup>1</sup> · Yuan Hu<sup>1</sup> · Wenru Zeng<sup>1</sup>

Received: 7 September 2018 / Accepted: 17 December 2019 / Published online: 11 January 2020  
© Akadémiai Kiadó, Budapest, Hungary 2020

## Abstract

We investigated the thermal decomposition behaviors of two typical grains, rice and corn, using a thermogravimetric analyzer at different heating rates. The pyrolysis process of rice and corn both can be divided into three stages, and the most possible pyrolysis mechanism of both rice and corn during devolatilization is a three-dimensional diffusion reaction, which can be represented by the Zhuravlev equation ( $G(\alpha) = [(1 - \alpha)^{-1/3} - 1]^2$ ). Corn had a higher initial degradation temperature and end temperature as well as a higher mass loss in the second stage than rice. The average  $E_a$  of rice determined by Kissinger, FWO and Friedman method was 143.6 kJ mol<sup>-1</sup>, 161.6 kJ mol<sup>-1</sup> and 148.7 kJ mol<sup>-1</sup>, respectively. The average  $E_a$  of corn determined by Kissinger, FWO and Friedman method was 166.1 kJ mol<sup>-1</sup>, 146.3 kJ mol<sup>-1</sup> and 170.4 kJ mol<sup>-1</sup>, respectively. A lower  $E_a$  of rice than corn also indicates that rice is easier to be pyrolyzed. The predicted values using the kinetic parameters calculated show a good agreement with the experimental data at all the four heating rates. The results presented herein could provide guidance for storage of grains.

**Keywords** Rice · Corn · Pyrolysis · Kinetics · Thermogravimetric analysis

## Introduction

Grain is an important strategic commodity closely related to the national economy and people's livelihood. With China joining the WTO and the gradual opening up of the grain market, the storage of large amounts of grains plays a vital

role to stabilize the development of the national economy. However, the amount of grain loss during storage is shocking. The annual loss of grains in China, caused by insects, rodents, mildew and fire accidents, is as high as 35 billion kilograms. For example, in 2013, the "5·31" fire accident ruined 40,000 tons grains that belonged to China Grain Reserves Corporation, leading to a direct economic loss of approximately 1 billion RMB. Therefore, how to avoid the grain loss during storage is a challenging task.

Among various grains, rice and corn are two kinds of the most common grains. Rice is the main food for more than half of the world's population, especially in developing countries in Asia, for which rice provides more than 70% of the daily caloric intake from foods [1]. As well, global corn production began to exceed that of rice and wheat in 1998, making it the world's highest-yielding, most productive food crops [2]. For example, the production of Chinese corn in the 2016/2017 season is 225,000 kt, and China is the second largest corn producer in the world. Corn is an important food crop in China and an important feed, which is one of the crops accounts for a considerable proportion of agricultural production in China. Thus, rice and corn are the top two grains in the China Grain Reserves list.

✉ Yuan Hu  
yuanhu@ustc.edu.cn

✉ Wenru Zeng  
wrzeng@ustc.edu.cn

Congxue Yao  
yaocx@mail.ustc.edu.cn

Xin Wang  
wxcmx@ustc.edu.cn

Yifan Zhou  
1509622771@qq.com

Xin Jin  
jinzhong@mail.ustc.edu.cn

Lei Song  
leisong@ustc.edu.cn

<sup>1</sup> State Key Laboratory of Fire Science, University of Science and Technology of China, Hefei 230027, Anhui, People's Republic of China

The initial stage of a fire generally begins with pyrolysis and ignition of combustibles, so studying the mechanism of grain pyrolysis is important for predicting fire occurrence and fire protection technology design [3]. Grain is composed of biomass rich in starch, protein, fat and a small amount of cellulose. Biomass pyrolysis and ignition are very complex physical and chemical processes, and many reviews have been introduced to analyze these processes comprehensively. Yang used a thermogravimetric analyzer combined with differential scanning calorimetry to study the pyrolysis characteristics of three major components of biomass (hemicellulose, cellulose and lignin) [4]. Pyrolysis of hemicellulose and cellulose occurs very quickly. The mass loss of hemicellulose occurs mainly at 220–315 °C, and the mass loss of cellulose occurs at 315–400 °C. Through in-depth study of the three major biomass components, a better understanding of the gaseous products released by biomass thermal interpretation can be obtained. Liu et al. [5] provide an overview of research progress in the discharge, conversion and distribution of elements in biomass pyrolysis, discuss resource-oriented transformation and the challenges of reducing pollution and emphasize the importance of understanding the fate of elements in pyrolysis and significance. Wu studied the pyrolysis behavior of fertilizers by TG. Results showed that the pyrolysis and combustion reactions were divided into four steps. The second step was the most critical step in which cellulose, hemicellulose, starch and protein were produced [6]. The relationship between co-pyrolysis municipal solid waste and pulp sludge and additives (MgO) was studied by TG-FTIR and Py-GC/MS. The release characteristics of pollutants (CO, SO<sub>2</sub>, NO, HCl) and CO<sub>2</sub> were studied in this literature [7].

Biomass pyrolysis is a very important way for us to know more about pyrolysis characteristics of biomass, which can provide theoretical guidance for grains storage to avoid fires. TGA has been widely used to investigate pyrolysis characteristics of different biomass and polymers [8–10]. TG data can be analyzed by many dynamic models, such as KAS method [11], Flynn–Wall–Ozawa (FWO) method [12] and Friedman (FR) method [13]. Rice and corn are the two typical grains in China. As far as we know, there is no research on the pyrolysis characteristics of rice and corn. Therefore,

we aimed to study the pyrolysis characteristics of rice and corn and to understand their kinetics characteristics. This will provide theoretical guidance for avoiding fires of rice and corn.

## Materials and methods

### Materials

The rice and corn were produced in Anhui province (2016), China. Rice was not yet removed rice husk, and the corn is the state of corn kernels. They were broken down to particles, and we got rice powder and corn powder. The materials were screened to get particles (250–400 μm), which is important for TGA to ensure a more consistent heat transfer rate in decomposition [14]. Table 1 shows the proximate and ultimate analyses result of the two powders. Moisture and volatility tests were carried out according to GB/T 28731-2012.

### Pyrolysis characteristics

The pyrolysis behaviors of rice and corn were studied using a TA Q50 thermogravimetric analyzer. The processed samples were heated in nitrogen atmosphere from room temperature to 800 °C at a heating rate of 5, 10, 20 and 40 °C min<sup>-1</sup>, respectively. The initial mass of the sample was 10 mg to avoid possible adverse effects on mass transfer or heat transfer during the test [15].

### Kinetic models

The one-step global kinetic model of biomass pyrolysis assumes that pyrolysis is a single reaction. The decomposition rate is expressed as follows:

$$\frac{d\alpha}{dt} = kf(\alpha) \quad (1)$$

where  $k$  is the reaction rate constant and  $f(\alpha)$  is the pyrolysis mechanism function.

**Table 1** Ultimate and proximate analyses result of rice and corn samples

Sample	Ultimate analysis					Proximate analysis			
	C	H	O	N	S	Moisture/%	Ash/%	Volatiles/%	Fixed carbon/%
Rice powder	44.88	6.85	47.84	2.19	0.23	12.09	3.92	73.24	10.75
Corn powder	41.93	6.91	49.97	1.43	0.29	12.25	1.24	75.95	10.56

Equation (1) expresses the rate of conversion,  $d\alpha/dt$  at a constant temperature as a function of the reactant conversion loss and rate constant. In this study, the conversion rate  $\alpha$  is defined as follows:

$$\alpha = \frac{m_0 - m_t}{m_0 - m_f} \tag{2}$$

in which  $m_0$  is the initial mass,  $m_t$  is the actual mass at time  $t$ , and  $m_f$  is the final mass.  $k$  is described as follows:

$$k = A \exp\left(\frac{-E_a}{RT}\right) \tag{3}$$

where  $R$  is the gas constant,  $E_a$  is the apparent activation energy,  $T$  is the absolute temperature, and  $A$  is the pre-exponential factor.

We can get Eq. (4) by combining Eqs. (1) and (3):

$$\frac{d\alpha}{dt} = A \exp\left(\frac{-E_a}{RT}\right) f(\alpha). \tag{4}$$

For a TG process, combining the heating rate,  $\beta = dT/dt$ , with Eq. (4), Eq. (5) is obtained as:

$$\frac{d\alpha}{dT} = \frac{A}{\beta} \exp\left(\frac{-E_a}{RT}\right) f\alpha. \tag{5}$$

Equations (4) and (5) can be used to calculate kinetics parameters based on TG data. By combining Eqs. (1) and (5) together using Coats–Redfern method, we can obtain Eq. (6):

$$\ln \frac{G(\alpha)}{T^2} = \ln \frac{AR}{\beta E} - \frac{E_a}{RT} \tag{6}$$

in which,

$$G(\alpha) = \int_0^\alpha \frac{d\alpha}{f(\alpha)}. \tag{7}$$

By linear fitting of  $\ln \frac{G(\alpha)}{T^2} \sim 1/T$  curve, the kinetic parameters  $A$  and  $E_a$  can be obtained from the intercept and slope of the line. By selecting different  $G(\alpha)$ , we can get different  $\ln \frac{G(\alpha)}{T^2} \sim 1/T$  curves, and from the linear correlation coefficient of the fitted line, we can get the appropriate mechanism function  $f(\alpha)$  and  $G(\alpha)$ . The general mechanism functions for thermal decomposition reaction of solid are list in Table 2.

Three non-isothermal models (FWO method, Friedman method and Kissinger method) were used in our study [16].

**Table 2** General mechanism functions for thermal decomposition reaction of solid

Model	$G(\alpha)$	$f(\alpha)$	Reaction mechanism
<i>Chemical reaction</i>			
F1	$-\ln(1 - \alpha)$	$1 - \alpha$	$n = 1$ reaction
F3/2	$2\left[(1 - \alpha)^{-\frac{1}{2}} - 1\right]$	$(1 - \alpha)^{\frac{3}{2}}$	$n = 1.5$ reaction
F2	$(1 - \alpha)^{-1} - 1$	$(1 - \alpha)^2$	$n = 2$ reaction
<i>Diffusion control reaction</i>			
D1	$\alpha^2$	$1/2 \alpha$	One-dimensional diffusion, Parabolic law
D2	$(1 - \alpha) \ln(1 - \alpha) + \alpha$	$-\ln(1 - \alpha)^{-1}$	Two-dimensional diffusion, Valensi equation
D3	$\left[1 - (1 - \alpha)^{1/3}\right]^2$	$1.5(1 - \alpha)^{2/3} \left[1 - (1 - \alpha)^{1/3}\right]^{-1}$	Three-dimensional diffusion, Jander equation
G-B	$(1 - 2/3\alpha) - (1 - \alpha)^{\frac{2}{3}}$	$1.5\left[(1 - \alpha)^{-\frac{1}{3}} - 1\right]^{-1}$	Three-dimensional diffusion, Ginstling–Broushtein equation
ZH	$\left[(1 - \alpha)^{-\frac{1}{3}} - 1\right]^2$	$1.5(1 - \alpha)^{4/3} \left[(1 - \alpha)^{-\frac{1}{3}} - 1\right]^{-1}$	Three-dimensional diffusion, Zhuravlev equation
<i>Phase boundary reaction</i>			
R1	$\alpha$	1	One-dimensional
R2	$1 - (1 - \alpha)^{1/2}$	$2(1 - \alpha)^{\frac{1}{2}}$	Two-dimensional, shrinking cylinder
R3	$1 - (1 - \alpha)^{1/3}$	$3(1 - \alpha)^{\frac{2}{3}}$	Three-dimensional, shrinking sphere
<i>Nucleation and growth</i>			
A2	$[-\ln(1 - \alpha)]^{1/2}$	$2(1 - \alpha)[- \ln(1 - \alpha)]^{1/2}$	Randomized nucleation, Avrami–Erofeev equation 1
A3	$[-\ln(1 - \alpha)]^{1/3}$	$3(1 - \alpha)[- \ln(1 - \alpha)]^{2/3}$	Randomized nucleation, Avrami–Erofeev equation 2

### Kissinger method [17]

The Kissinger equation is a classic nonnuclear kinetic equation widely used in the calculation of activation energy and pre-exponential factor [17, 18]. The advantage of this algorithm is that it does not require a blind selection of the mechanism model during the calculation [19]. The equation is shown in Eq. (8):

$$\ln \frac{\beta}{T_{\max}^2} = \ln \frac{AR}{E_a} - \frac{E_a}{RT_{\max}} \quad (8)$$

where  $T_{\max}$  is peak decomposition temperature.

By linear fitting of  $\ln \frac{\beta}{T_{\max}^2}$  to  $\frac{1}{T_{\max}}$  curve,  $A$  and  $E_a$  can be obtained from the intercept and the slope, respectively.

### FWO method

The FWO method [20, 21] can directly solve for  $E_a$ , and there are two methods for solving the  $E_a$ , namely the approximate conversion method for peak conversion and the equal conversion method. The equation is shown in Eq. (9):

$$\lg \beta = \lg \left[ \frac{AE}{RG(\alpha)} \right] - 0.4567 \frac{E}{RT_{\alpha}} - 2.315 \quad (9)$$

in which  $G(\alpha)$  is integral kinetic mechanism function and  $T_{\alpha}$  is the temperature where the conversion rate is  $\alpha$ . By linear fitting of  $\ln \beta$  to  $\frac{1}{T_{\alpha}}$ ,  $A$  and  $E_a$  can be obtained from the intercept and the slope, respectively.

### Friedman method [22]

The equation of Friedman method is shown in Eq. (10):

$$\ln \left( \frac{d\alpha}{dt} \right) = \ln \left( \beta \frac{d\alpha}{dT} \right) = \ln (Af(\alpha)) - \frac{E}{RT}. \quad (10)$$

By linear fitting of  $\ln \left( \beta \frac{d\alpha}{dT} \right)$  to  $\frac{1}{T}$ ,  $A$  and  $E_a$  can be obtained from the intercept and the slope, respectively.

## Results and discussion

### Pyrolysis characteristics of rice

TG and DTG curves of rice in nitrogen atmosphere at different heating rates ( $5 \text{ }^{\circ}\text{C min}^{-1}$ ,  $10 \text{ }^{\circ}\text{C min}^{-1}$ ,  $20 \text{ }^{\circ}\text{C min}^{-1}$ ,  $40 \text{ }^{\circ}\text{C min}^{-1}$ ) are shown in Fig. 1.

The main decomposition process of rice occurs in a temperature range of  $200 \text{ }^{\circ}\text{C}$  to  $500 \text{ }^{\circ}\text{C}$ . Due to the large amount of ash and fixed carbon in rice, there is about 20 mass% of residual carbon after TG analysis. From TG and DTG curves of rice, the pyrolysis process of rice can be divided into three

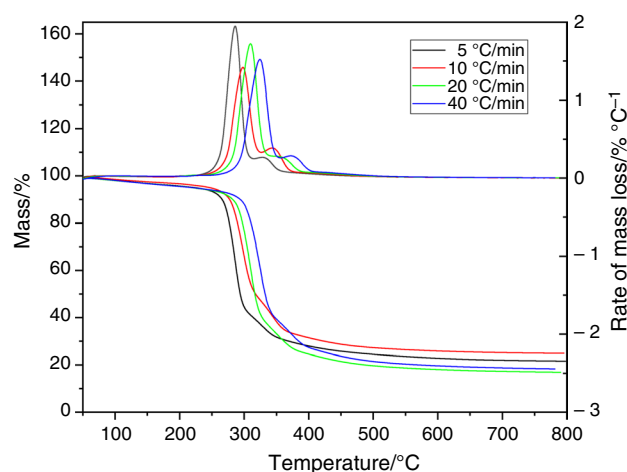


**Fig. 1** TG and DTG curves of rice at different heating rates in nitrogen atmosphere

stages, and the temperature regions are: (1) under  $200 \text{ }^{\circ}\text{C}$ , (2)  $200\text{--}500 \text{ }^{\circ}\text{C}$ , and (3) over  $500 \text{ }^{\circ}\text{C}$ . Table 3 shows the pyrolysis characteristics of rice in different pyrolysis stages.

In the first stage of decomposition, the moisture in the rice, mainly including free water, crystal water and adsorbed water, was lost [23]. Free water and the adsorbed water were lost at a lower temperature, and then, the crystal water was removed at a higher temperature.

In the second stage, the pyrolysis reaction of rice mainly occurred and the mass loss was nearly 60%. The peak temperature of the maximum mass loss rate is  $286 \text{ }^{\circ}\text{C}$ ,  $297 \text{ }^{\circ}\text{C}$ ,  $310 \text{ }^{\circ}\text{C}$  and  $324 \text{ }^{\circ}\text{C}$  corresponding to a heating rate of 5, 10, 20 and  $40 \text{ }^{\circ}\text{C min}^{-1}$ . As the heating rate increased, its heat transfer delay effect became more obvious and TG and DTG curves of the rice sample showed the tendency to move to the high temperature side in nitrogen atmosphere. In the second stage, we can see two peaks on the DTG curves, which is consistent with the results of previous studies. The first exothermic peak is mainly due to the decomposition of carbohydrates, and the second exothermic peak is due to the decomposition and secondary cracking of the pyrolyzates of proteins, lipids and cellulose [24]. Cellulose decomposes at the temperature range between  $320$  and  $380 \text{ }^{\circ}\text{C}$ .

In the third stage, the mass loss is mainly due to the thermal degradation process of tar or char residue. The rearrangement of the starch structure at the low temperature promoted the production of char residue.

Many literatures also reported that the composition of various biomasses is not the same, and their pyrolysis behavior varies from species to species [25]. Therefore, it is impossible to define each decomposition temperature zone as the decomposition temperature interval of a specific component (carbohydrate, lipid or protein), and each decomposition temperature zone must be analyzed according to the

**Table 3** Pyrolysis characteristics of rice

Heating rate/ $^{\circ}\text{C min}^{-1}$	1st stage			2nd stage					3rd stage		
	$T_i/^{\circ}\text{C}$	$T_p/^{\circ}\text{C}$	MS/%	$T_i/^{\circ}\text{C}$	$T_p/^{\circ}\text{C}$	$R_{\max}/\% \text{ } ^{\circ}\text{C}^{-1}$	$T_e/^{\circ}\text{C}$	MS/%	$T_i/^{\circ}\text{C}$	$T_e/^{\circ}\text{C}$	MS/%
5	55	266	5.9	266	286	1.4	312	59.4	312	800	12.7
10	55	269	4.8	269	297	1.5	327	57.8	327	800	11.1
20	55	284	7.2	284	310	1.7	336	64.4	336	800	10.4
40	55	300	7.9	300	324	1.9	349	60.9	349	800	11.9

$T_i$  is initial temperature;  $T_p$  is peak temperature corresponding to maximum mass loss rate;  $R_{\max}$  is the maximum mass loss rate;  $T_e$  is end temperature; MS is mass loss

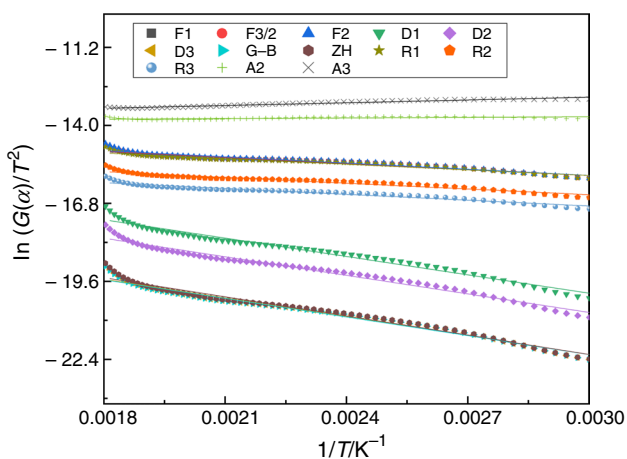


**Fig. 2**  $\ln \frac{G(\alpha)}{T^2} \sim 1/T$  of rice at low-temperature section 50–300  $^{\circ}\text{C}$

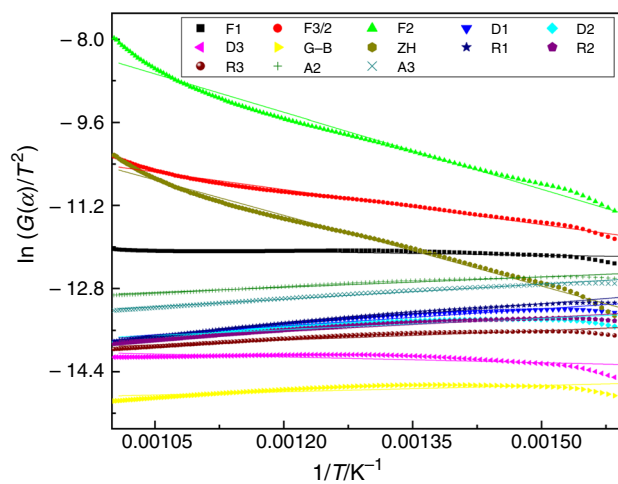


**Fig. 3**  $\ln \frac{G(\alpha)}{T^2} \sim 1/T$  of rice at high-temperature section 300–700  $^{\circ}\text{C}$

product analysis of each temperature zone, which will be investigated in our follow-up studies.

Figures 2 and 3 show  $\ln \frac{G(\alpha)}{T^2} \sim 1/T$  of rice at a low-temperature section and a high-temperature section at the heating rate of 20  $^{\circ}\text{C min}^{-1}$  for example. The fitting result of different curves is shown in Table 4.

From the fitting result of different  $\ln \frac{G(\alpha)}{T^2} \sim 1/T$  curves, we can find that at a low-temperature section, ZH model shows a Pearson's  $r$  that is very close to  $-1$ , and at a high-temperature section, ZH model also shows the best fitting result. Therefore, we can assume that the pyrolysis of rice is the diffusion reaction control process and the kinetic model of rice pyrolysis is ZH model. The mechanism function of ZH model is Eq. (11):

$$G(\alpha) = \left[ (1 - \alpha)^{-\frac{1}{3}} - 1 \right]^2 \tag{11}$$

### Pyrolysis characteristics of corn

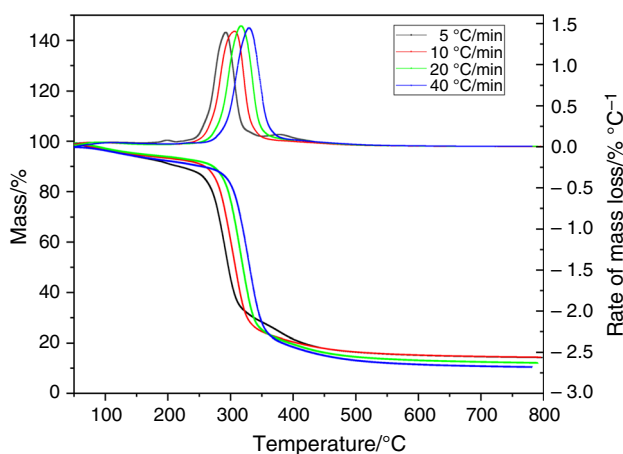
TG and DTG curves of corn in nitrogen atmosphere at different heating rates are shown in Fig. 4.

From Table 1, we can see that the rice powder has a higher content of ash and fixed carbon and lower content of moisture and volatiles than that of corn powder, which is consistent with the TG results—corn powder has more than 80% mass loss and rice powder has less than 80% mass loss, which can be seen from Figs. 1 and 4.

Just like rice, as the heating rate increases, its heat transfer delay effect became more obvious and TG and DTG curves of the corn sample show the tendency to move to the high temperature side in nitrogen atmosphere. During the pyrolysis process, the temperature gradient generated inside the corn leads to the formation of thermal hysteresis. The higher the heating rate, the more obvious the thermal hysteresis effect [26]. The pyrolysis process of corn also included three stages. Table 5 shows the pyrolysis characteristics of corn in three consecutive pyrolysis stages.

**Table 4** The fitting result of different  $\ln \frac{G(\alpha)}{T^2} \sim 1/T$  curves of rice

Low temperature (50–300 °C)							
$G(\alpha)$	F1	F3/2	F2	D1	D2	D3	G_B
Pearson's $r$	-0.9764	-0.9771	-0.9779	-0.9914	-0.9914	-0.9915	-0.9914
$G(\alpha)$	ZH	R1	R2	R3	A2	A3	
Pearson's $r$	-0.9916	-0.9745	-0.9755	-0.9758	0.61342	0.9757	
High temperature (300–700 °C)							
$G(\alpha)$	F1	F3/2	F2	D1	D2	D3	G_B
Pearson's $r$	-0.7528	-0.9923	-0.9908	0.9666	0.8877	-0.6792	0.7186
$G(\alpha)$	ZH	R1	R2	R3	A2	A3	
Pearson's $r$	-0.9957	0.9899	0.9641	0.9262	0.9778	0.9919	

**Fig. 4** TG and DTG curves of corn at different heating rates in nitrogen atmosphere

Similarly, from the TG and DTG curves of corn, we conclude that the pyrolysis process included three stages.

In the first stage of the reaction, the mass loss was mainly attributed to evaporation of the moisture in corn, including free water, adsorbed water and crystal water.

In the second stage, the pyrolysis reaction of rice mainly occurred. The mass loss was nearly 60% in this stage, which is similar to rice. The peak temperature of the maximum mass loss rate was 292 °C, 307 °C, 318 °C and 329 °C corresponding to the heating rates of 5, 10, 20, and 40 °C min<sup>-1</sup>. Compared to rice, corn showed higher peak temperature, about 5–10 °C higher than rice. In the second stage, we can also see two peaks on the DTG curves, which is similar to the results of rice. However, we can tell that the second peak of corn is almost invisible and the second peak of rice

is obvious. This can be explained by the difference in the composition of the main components of the two kinds of grain powder. Considering rice husk was not removed, the rice powder had much more cellulose than corn powder, which results in the above phenomenon.

In the third stage, the mass loss is also mainly due to the thermal degradation process of tar or char residue.

Figures 5 and 6 show  $\ln \frac{G(\alpha)}{T^2} \sim 1/T$  curves of corn at a low-temperature section and a high-temperature section at the heating rate of 20 °C min<sup>-1</sup>. The fitting result of different curves is shown in Table 6.

From the fitting result of different  $\ln \frac{G(\alpha)}{T^2} \sim 1/T$  curves, we can also assume that the pyrolysis of corn is the diffusion reaction control process and the kinetic model of corn pyrolysis is ZH model.

The diffusion-controlled reaction model, ZH model, assumes that the surface reaction rate depends on the rate at which the gaseous oxidant diffuses to the particle surface, and the effect of surface reaction kinetics is ignored. In the literature reported, we find that pine wood, sunflower stalk, coal powder and *Enteromorpha prolifera* (a kind of macroalgae) are three-dimensional diffusion process in their pyrolysis process.

As we all know, lignocellulosic biomass primarily comprises three components: hemicellulose, cellulose, and lignin. Rice and corn mainly contain starch, protein, lipid and cellulose. The components of rice and corn are different from the above lignocellulosic biomass, and there is no literature about their reaction models. It is interesting that the pyrolysis processes of rice and different biomass are all controlled by three-dimensional diffusion reaction, ZH model, though their composition are different. This may be related to the fact that they are all composed of complex natural polymer materials. The degradation processes of starch,

**Table 5** Pyrolysis characteristics of corn

Heating rate/ $^{\circ}\text{C min}^{-1}$	1st stage			2nd stage					3rd stage		
	$T_i/^{\circ}\text{C}$	$T_p/^{\circ}\text{C}$	MS/%	$T_i/^{\circ}\text{C}$	$T_p/^{\circ}\text{C}$	$R_{\max}/\% \text{ } ^{\circ}\text{C}^{-1}$	$T_e/^{\circ}\text{C}$	MS/%	$T_i/^{\circ}\text{C}$	$T_e/^{\circ}\text{C}$	MS/%
5	55	269	13.1	261	292	1.4	312	55.2	312	428	15.3
10	55	271	9.2	271	307	1.4	330	64.1	330	484	11.3
20	55	285	9.2	285	318	1.5	338	66.4	338	599	11.4
40	55	295	11.6	295	329	1.4	356	66.9	356	591	10.0

$T_i$  is initial temperature;  $T_p$  is peak temperature corresponding to maximum mass loss rate;  $R_{\max}$  is the maximum mass loss rate;  $T_e$  is end temperature; MS is mass loss

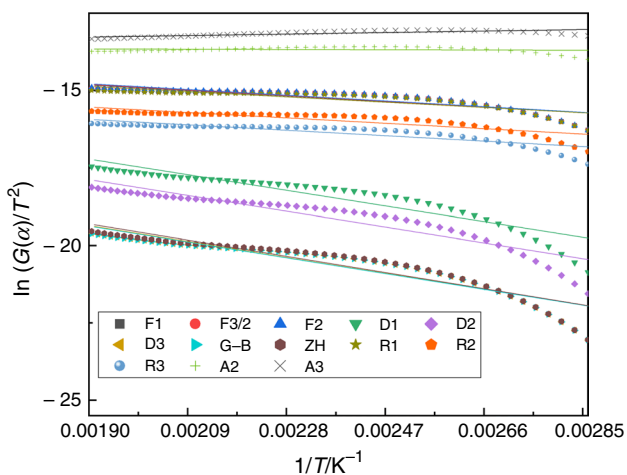
cellulose and hemicellulose are small molecule removal reactions, and the gaseous oxidant diffuse rate is much slower than the surface reaction rate, which results in the same reaction model of crops and lignocellulosic biomass.

### Kinetic models from three methods

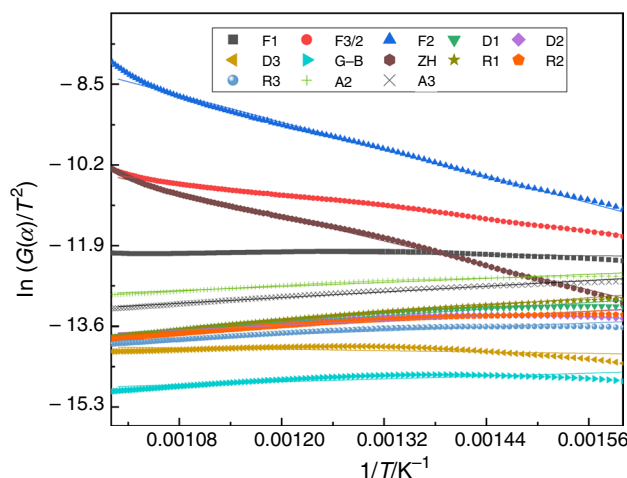
#### Kissinger method

Figure 7 shows the relationship between  $\ln \frac{\beta}{T_{\max}^2}$  and  $\frac{1}{T_{\max}}$  (Table 7).

Table 4 shows  $E_a$  of rice and corn at different conversion rates. The range of  $E_a$  of rice powder is between 141.7 and 145.5  $\text{kJ mol}^{-1}$ , and the average  $E_a$  is 143.6  $\text{kJ mol}^{-1}$ . The  $E_a$  of corn powder is 166.1  $\text{kJ mol}^{-1}$ . It is a common practice to represent the apparent  $E_a$  of biomass pyrolysis as an average to describe the overall process. Since  $E_a$  is the lowest energy requirement to initiate a reaction, the higher the  $E_a$ , the slower the reaction [27]. It can be seen that corn



**Fig. 5**  $\ln \frac{G(\alpha)}{T^2} \sim 1/T$  of corn at low-temperature section 50–300  $^{\circ}\text{C}$



**Fig. 6**  $\ln \frac{G(\alpha)}{T^2} \sim 1/T$  of corn at high-temperature section 300–700  $^{\circ}\text{C}$

has higher  $E_a$  (166.1  $\text{kJ mol}^{-1}$ ) than rice (143.6  $\text{kJ mol}^{-1}$ ), indicating that the energy required to complete rice pyrolysis is less than that of corn, and rice is more susceptible to pyrolysis.

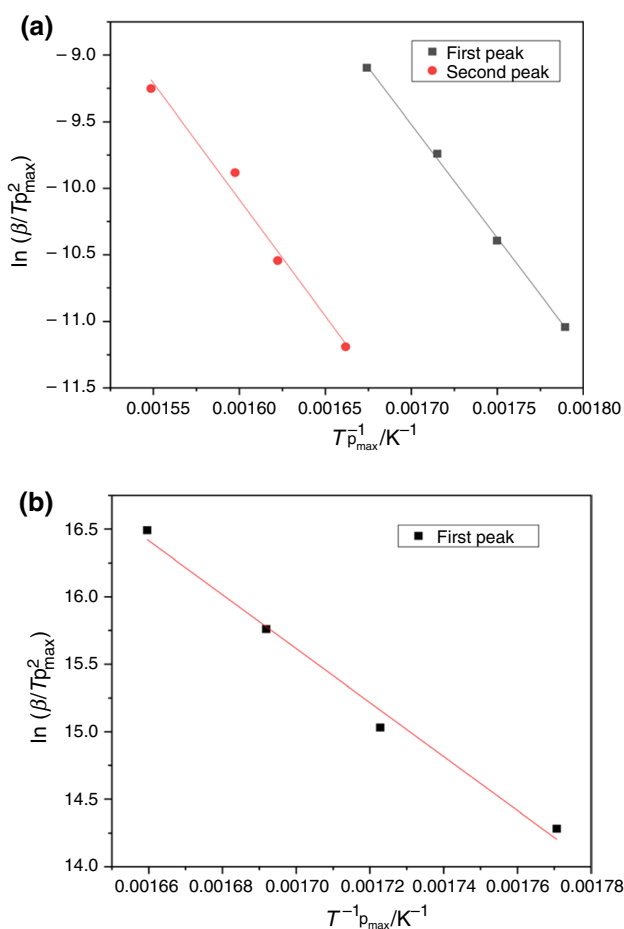
#### FWO method

Figure 8 shows the relationship between  $\lg \beta$  and  $\frac{1}{T_{\alpha}}$ .

Table 8 shows the  $E_a$  of rice and corn calculated by FWO method at different conversion rates. The range of apparent  $E_a$  of rice powder was between 141.7 and 219.7  $\text{kJ mol}^{-1}$ , and the average  $E_a$  is 161.6  $\text{kJ mol}^{-1}$ . The range of apparent  $E_a$  of corn powder was between 80.1 and 176.9  $\text{kJ mol}^{-1}$ , and the average  $E_a$  is 146.3  $\text{kJ mol}^{-1}$ . Consistent with the Kissinger results, it was also found that corn had higher  $E_a$  (161.6  $\text{kJ mol}^{-1}$ ) than rice (146.3  $\text{kJ mol}^{-1}$ ), suggesting that the required energy for the pyrolysis of rice was less than that of corn, and rice was easier to be pyrolyzed than corn.

**Table 6** The fitting result of different  $\ln(G(\alpha))/T^2 \sim 1/T$  curves of corn

Low temperature (50–300 °C)							
$G(\alpha)$	F1	F3/2	F2	D1	D2	D3	G_B
Pearson's r	-0.8661	-0.8702	-0.8741	-0.9308	-0.9319	-0.9330	-0.932
$G(\alpha)$	ZH	R1	R2	R3	A2	A3	
Pearson's r	-0.9350	-0.8574	-0.8618	-0.8633	-0.1430	0.7784	
High temperature (300–700 °C)							
$G(\alpha)$	F1	F3/2	F2	D1	D2	D3	G_B
Pearson's r	-0.5453	-0.9974	-0.9972	0.9752	0.9201	-0.5174	0.8084
$G(\alpha)$	ZH	R1	R2	R3	A2	A3	
Pearson's r	-0.9981	0.9916	0.9698	0.9391	0.9771	0.9911	

**Fig. 7** Non-isothermal plot of Kissinger method at different heating rates: **a** rice and **b** corn**Table 7** Pyrolysis kinetic parameters of Kissinger method

Sample	$E_a/kJ\ mol^{-1}$	Frequency factor/ $min^{-1}$	$R^2$
<i>Rice</i>			
First peak	141.7	4.74E+12	0.99894
Second peak	145.5	1.05E+12	0.98338
Average	143.6	—	—
<i>Corn</i>			
First peak	166.1	6.82E+25	0.98960
Average	166.1	—	—

### Friedman method

Here, the result of Friedman method is shown. Figure 9 shows the linear fitting curves of  $\ln\left(\beta\frac{d\alpha}{dT}\right)$  to  $\frac{1}{T}$ .

Table 9 shows the  $E_a$  of rice and corn calculated by Friedman method at different conversion rates. The range of apparent  $E_a$  of rice powder was between 127.8 and 220.8  $kJ\ mol^{-1}$ , and the average  $E_a$  is 148.7  $kJ\ mol^{-1}$ . The range of apparent  $E_a$  of corn powder was between 121.7 and 221.7  $kJ\ mol^{-1}$ , and the average  $E_a$  is 170.4  $kJ\ mol^{-1}$ .

It can be seen from Fig. 10 and Table 10 that the  $E_a$  of corn increased with the increase in conversion rate, while the  $E_a$  of rice fluctuates with the increase in conversion rate, which are similar to those of FWO method. We compared the results of the  $E_a$  of rice and corn calculated by the three methods, as shown in Fig. 10. The  $E_a$  calculated by the three methods is very close, and the maximum relative error is less than 0.21, which demonstrated that the methods adopted and

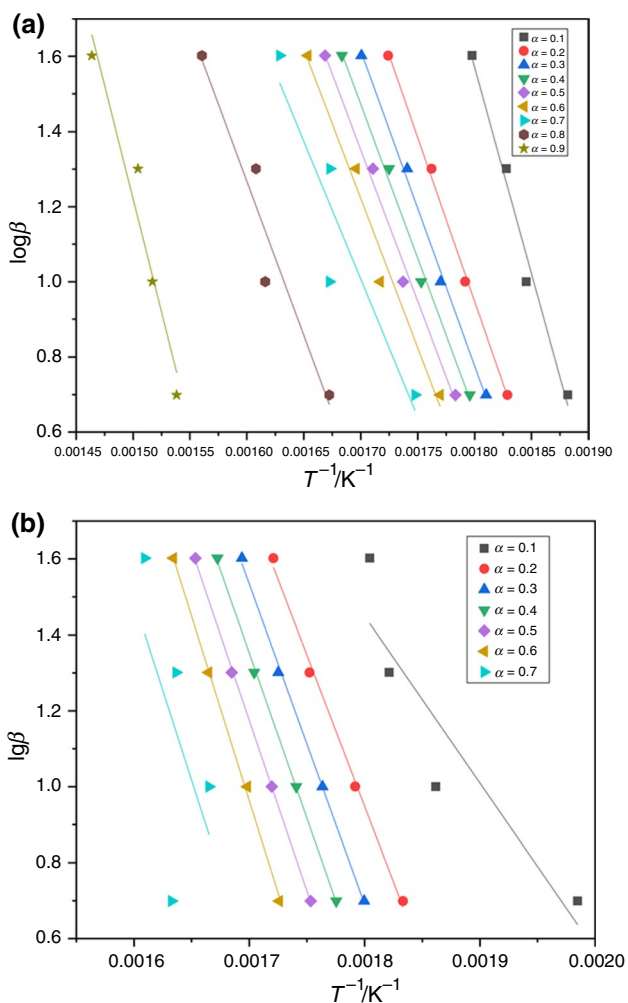


**Fig. 8** Non-isothermal plot of FWO method at different heating rates: **a** rice and **b** corn

values are credible. It can be seen that the  $E_a$  of rice calculated by FWO method increased greatly from 149 kJ mol<sup>-1</sup> ( $\alpha=0.8$ ) to 219 kJ mol<sup>-1</sup> ( $\alpha=0.9$ ), and the  $E_a$  of rice calculated by Friedman method increased from 161 kJ mol<sup>-1</sup>

**Table 8** Pyrolysis kinetic parameters of FWO method

Sample	Conversion rate $\alpha$	$E_a$ /kJ mol <sup>-1</sup>	Frequency factor/min <sup>-1</sup>	$R^2$
Rice	0.1	200.2	2.52E+16	0.98338
	0.2	159	2.98E+12	0.99781
	0.3	152.7	1.34E+12	0.9964
	0.4	149.1	9.89E+11	0.99422
	0.5	146.6	8.78E+11	0.99043
	0.6	144.6	8.11E+11	0.97634
	0.7	133.5	9.30E+10	0.86782
	0.8	149.3	1.41E+12	0.93622
	0.9	219.7	2.18E+17	0.94614
	Average	161.6	–	–
Corn	0.1	80.1	6.44E+04	0.84906
	0.2	145	1.36E+11	0.99618
	0.3	153.5	1.31E+12	0.99853
	0.4	158.5	5.29E+12	0.99935
	0.5	163.6	2.02E+13	0.9996
	0.6	176.9	3.73E+14	0.9988
	Average	146.3	–	–

( $\alpha=0.8$ ) to 221 kJ mol<sup>-1</sup> ( $\alpha=0.9$ ), which can be attributed to devolatilization of charcoal from rice [28].

Vamvuka et al. [29] studied the pyrolysis characteristics of biomass residual mixtures with lignite. The kinetics of the thermal decomposition were modeled by a scheme consisting of three independent first-order parallel reactions of the main biopolymer components: hemicellulose, cellulose and lignin. They reported  $E_a$  values between 145 kJ mol<sup>-1</sup> and 285 kJ mol<sup>-1</sup> for cellulose, 90 kJ mol<sup>-1</sup> and 125 kJ mol<sup>-1</sup> for hemicellulose and 30 kJ mol<sup>-1</sup> and 39 kJ mol<sup>-1</sup> for lignin. Xue et al. [30] studied the pyrolysis characteristics of cellulose, starch and mixtures of different content of cellulose and starch. Their result showed that the  $E_a$  value of cellulose is between 105 kJ mol<sup>-1</sup> and 169 kJ mol<sup>-1</sup> and the  $E_a$  value of starch is between 197 and 271 kJ mol<sup>-1</sup>, which is related

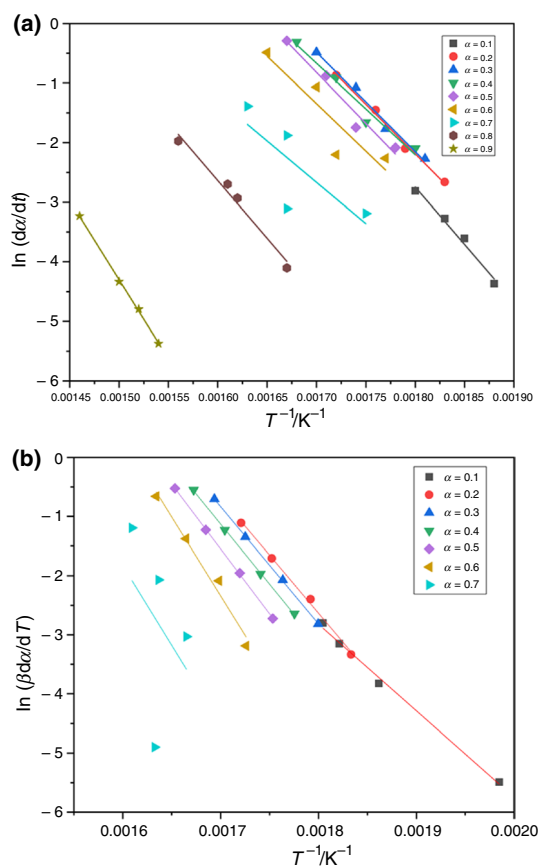


**Fig. 9** Non-isothermal plot of Friedman method at different heating rates: **a** rice and **b** corn

**Table 9** Pyrolysis kinetic parameters of Friedman method

Sample	Conversion rate	$E_a/kJ mol^{-1}$	Frequency factor/ $min^{-1}$	$R^2$
Rice	0.1	160.5	2.17E+12	0.98213
	0.2	138.4	8.05E+10	0.99321
	0.3	138.7	1.74E+11	0.98866
	0.4	127.8	2.82E+10	0.96377
	0.5	142.6	8.87E+11	0.95821
	0.6	132.4	1.20E+11	0.82033
	0.7	115.4	2.02E+09	0.59271
	0.8	161.2	8.47E+12	0.97812
	0.9	220.8	4.51E+16	0.99892
	Average	148.7	–	–
Corn	0.1	121.7	4.51E+08	0.9954
	0.2	163.1	1.07E+13	0.99668
	0.3	164.6	2.46E+13	0.99974
	0.4	168.8	7.70E+13	0.99967
	0.5	182.2	1.40E+15	0.99976
	0.6	221.7	3.82E+18	0.97917
	Average	170.4	–	–

to conversion. Their research also showed that blending may promote devolatilization, seen through lower  $E_a$ . Our research object, rice and corn are mixture of starch, protein, lipid, cellulose and many other chemicals, which are more complicated than the single component. The  $E_a$  of rice and corn calculated by three different methods is very close to the above literature.

As shown in Fig. 11, the predicted values using the kinetic parameters calculated show a good agreement with the experimental data at all heating rates. The high agreement indicates that our pyrolysis kinetic parameters are reliable.

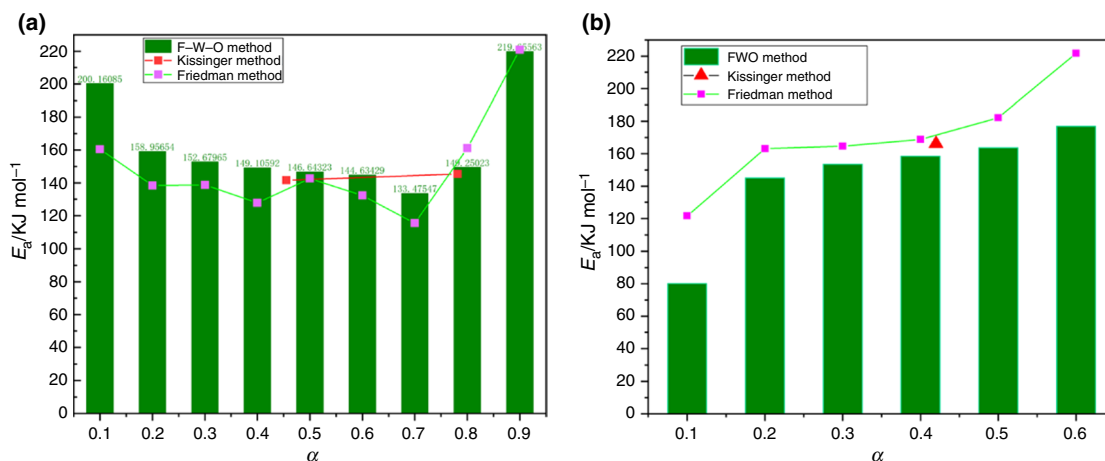
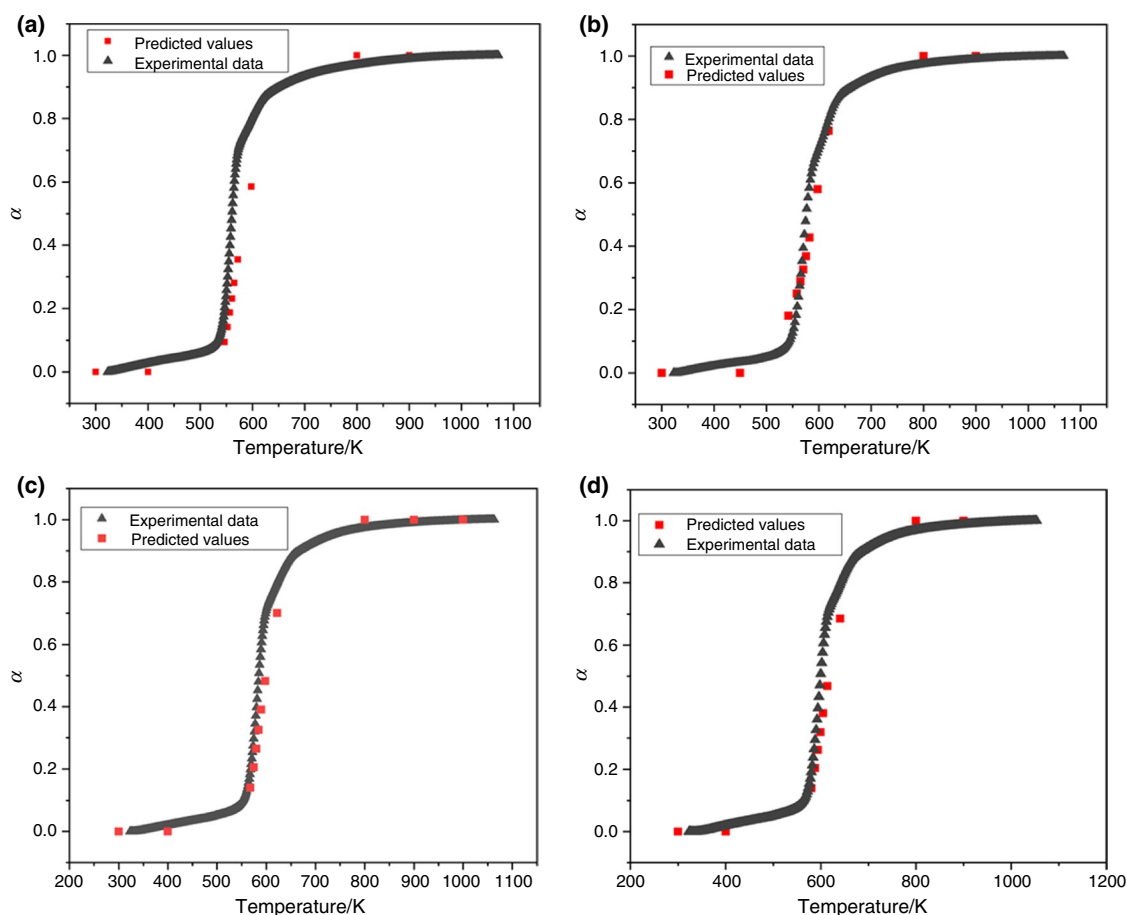


Fig. 10 Comparison of  $E_a$  calculated by Kissinger method, FWO method and Friedman method at different conversion: **a** rice and **b** corn

**Table 10** Comparison of  $E_a$  of rice and corn calculated by three methods

Sample	$\alpha$	Kissinger $E_a/$ $\text{kJ mol}^{-1}$	FWO $E_a/\text{kJ mol}^{-1}$	Friedman $E_a/$ $\text{kJ mol}^{-1}$	Average $E_a/$ $\text{kJ mol}^{-1}$	Maximum relative error
Corn	0.1		80.1	121.7	100.9	0.21
	0.2		145.0	163.1	154.0	0.06
	0.3		153.5	164.6	159.1	0.04
	0.4	166.1	158.5	168.8	164.4	0.04
	0.5		163.6	182.2	172.9	0.05
	0.6		176.9	221.7	199.3	0.11
Rice	0.1		200.2	160.5	180.3	0.11
	0.2		159.0	138.4	148.7	0.07
	0.3		152.7	138.7	145.7	0.05
	0.4		149.1	127.8	138.5	0.08
	0.5	141.7	146.6	142.6	143.6	0.02
	0.6		144.6	132.4	138.5	0.04
	0.7		133.5	115.4	124.4	0.07
	0.8	145.5	149.3	161.2	152.0	0.06
	0.9		219.7	220.8	220.2	0.00



**Fig. 11** Comparison between experimental and predicted values at different heating rates: **a** 5 °C min<sup>-1</sup>, **b** 10 °C min<sup>-1</sup>, **c** 20 °C min<sup>-1</sup> and **d** 40 °C min<sup>-1</sup>

## Conclusions

In this study, the pyrolysis characteristics of two typical grains, rice and corn, were investigated and modeled from thermogravimetric analysis, where three decomposition stages were observed. With heating rates increasing, the temperature at the maximum mass loss rate shifted to a higher temperature. Compared to rice, corn had a higher initial decomposition temperature and end temperature under different heating rates in their main pyrolysis stage. The most possible pyrolysis mechanism during devolatilization is three-dimensional diffusion, which can be represented by the Zhuravlev equation ( $G(\alpha) = [(1 - \alpha)^{-1/3} - 1]^2$ ). Lower  $E_a$  of rice than corn also indicates that rice is easier to be pyrolyzed. The predicted values using the kinetic parameters calculated show a good agreement with the experimental data at all the heating rates. The developed kinetics characteristics can be employed for grain pyrolysis prediction and grain reserves.

**Acknowledgements** The authors would like to acknowledge the support from National Key Research and Development Program of China (2017YFC0805900) and Fundamental Research Funds for the Central Universities (WK2320000041 and WK2320000043).

## References

1. Xiao G, Yingli H, Li N, Yang D. Spatial autocorrelation analysis of monitoring data of heavy metals in rice in China. *Food Control*. 2018;89:32–7. <https://doi.org/10.1016/j.foodcont.2018.01.032>.
2. Yang H, Han X. Comparison of corn production, trade, consumption and storage among main producing countries: based on 1996/1997–2016/2017 production season. *World Agric*. 2017. <https://doi.org/10.13856/j.cn11-1097/s.2017.06.005>.
3. Wang Y, Zheng X. Modeling and experimental study of the effect of pressure on pyrolysis of wet wood. *J Fire Sci*. 2013;31:495–510. <https://doi.org/10.1177/0734904113482104>.
4. Yang H, Yan R, Chen H, Lee DH, Zheng C. Characteristics of hemicellulose, cellulose and lignin pyrolysis. *Fuel*. 2007;86:1781–8. <https://doi.org/10.1016/j.fuel.2006.12.013>.

5. Liu W-J, Li W-W, Jiang H, Yu H-Q. Fates of chemical elements in biomass during its pyrolysis. *Chem Rev.* 2017;117:6367–98. <https://doi.org/10.1021/acs.chemrev.6b00647>.
6. Wu H, Hanna MA, Jones DD. Thermogravimetric characterization of dairy manure as pyrolysis and combustion feedstocks. *Waste Manag Res.* 2012;30(10):1066–71. <https://doi.org/10.1177/0734242X12452906>.
7. Fang S, Yu Z, Ma X, Lin Y, Chen L, Liao Y. Analysis of catalytic pyrolysis of municipal solid waste and paper sludge using TG-FTIR, Py-GC/MS and DAEM (distributed activation energy model). *Energy.* 2018;143:517–32. <https://doi.org/10.1016/j.energy.2017.11.038>.
8. Correia LP, de Santana CP, da Silva KMA. Physical and chemical characteristics of *Maytenus rigida* in different particle sizes using SEM/EDS, TG/DTA and pyrolysis GC–MS. *J Therm Anal Calorim.* 2018;131:743–52. <https://doi.org/10.1007/s10973-016-5999-0>.
9. Zhu F, Yanfang X, Feng Q, Yang Q. Thermal kinetics study and flammability evaluation of polyimide fiber material. *J Therm Anal Calorim.* 2018;1131:2579–87. <https://doi.org/10.1007/s10973-017-6752-z>.
10. Rath J, Steiner G, Wolfinger MG. Tar cracking from fast pyrolysis of large beech wood particles. *J Anal Appl Pyrolysis.* 2002;62:83–92. [https://doi.org/10.1016/S0165-2370\(00\)00215-1](https://doi.org/10.1016/S0165-2370(00)00215-1).
11. Branca C, Di Blasi C. A unified mechanism of the combustion reactions of lignocellulosic fuels. *Thermochim Acta.* 2013;565:58–64. <https://doi.org/10.1016/j.tca.2013.04.014>.
12. Ozawa T. A new method of analyzing thermogravimetric data. *Bull Chem Soc Jpn.* 1965;38:1881–6. <https://doi.org/10.1246/bcsj.38.1881>.
13. Friedman HL. New methods for evaluating kinetic parameters from thermal analysis data. *J Polym Sci Polym Chem.* 1969;7:41–6. <https://doi.org/10.1002/pol.1969.110070109>.
14. Garcia-Maraver A, Perez-Jimenez JA, Serrano-Bernardo F, Zamorano M. Determination and comparison of combustion kinetics parameters of agricultural biomass from olive trees. *Renew Energy.* 2015;83:897–904. <https://doi.org/10.1016/j.renene.2015.05.049>.
15. Mani T, Murugan P, Abedi J, Mahinpey N. Pyrolysis of wheat straw in a thermogravimetric analyzer: effect of particle size and heating rate on devolatilization and estimation of global kinetics. *Chem Eng Res Des.* 2010;88:952–8. <https://doi.org/10.1016/j.cherd.2010.02.008>.
16. Anca-Couce A, Berger A, Zobel N. How to determine consistent biomass pyrolysis kinetics in a parallel reaction scheme. *Fuel.* 2014;123:230–40. <https://doi.org/10.1016/j.fuel.2014.01.014>.
17. Starink MJ. The determination of activation energy from linear heating rate experiments: a comparison of the accuracy of iso-conversion methods. *Thermochim Acta.* 2003;404:163–76. [https://doi.org/10.1016/S0040-6031\(03\)00144-8](https://doi.org/10.1016/S0040-6031(03)00144-8).
18. Maraden A, Stojan P, Matyas R, Zigmund J. Impact of initial grain temperature on the activation energy and the burning rate of cast double-base propellant. *J Therm Anal Calorim.* 2019;137:185–91. <https://doi.org/10.1007/s10973-018-7927-y>.
19. Magdziarz A, Wilk M, Straka R. Combustion process of torrefied wood biomass. *J Therm Anal Calorim.* 2017;127:1339–49. <https://doi.org/10.1007/s10973-016-5731-0>.
20. Slopiecka K. Thermogravimetric analysis and kinetic study of poplar wood pyrolysis. *Appl Energy.* 2012;97:491–7. <https://doi.org/10.1016/j.apenergy.2011.12.056>.
21. Dogan F, Ozdek N, Selçuki NA, Kaya I. The synthesis, characterization and effect of molar mass distribution on solid-state degradation kinetics of oligo(orcino). *J Therm Anal Calorim.* 2019;138:163–73. <https://doi.org/10.1007/s10973-019-08211-x>.
22. Baas IO, Mulder J-WR, Offerhaus GJA, Vogelstein B, Hamilton SR. An evaluation of six antibodies for immunohistochemistry of mutant p53 gene product in archival colorectal neoplasms. *J Pathol.* 1994;172:5–12. <https://doi.org/10.1002/path.1711720104>.
23. Whitea JE, Catalo WJ, Legendrea BL. Biomass pyrolysis kinetics: a comparative critical review with relevant agricultural residue case studies. *J Anal Appl Pyrolysis.* 2011;91:1–33. <https://doi.org/10.1016/j.jaap.2011.01.004>.
24. Kim Y-M. Analytical pyrolysis reaction characteristics of *Porphyra tenera*. *Algal Res.* 2018;32:60–9. <https://doi.org/10.1016/j.algal.2018.03.003>.
25. Anastasakis K, Ross A. Pyrolysis behaviour of the main carbohydrates of brown macro-algae. *J. Jones Fuel.* 2011;90:598–607. <https://doi.org/10.1016/j.fuel.2010.09.023>.
26. Agrawal A, Chakraborty S. A kinetic study of pyrolysis and combustion of microalgae *Chlorella vulgaris* using thermo-gravimetric analysis. *Bioresour Technol.* 2013;128:72–80. <https://doi.org/10.1016/j.biortech.2012.10.043>.
27. Ceylan S, Topçu Y. Pyrolysis kinetics of hazelnut husk using thermogravimetric analysis. *Bioresour Technol.* 2014;156:182–8. <https://doi.org/10.1016/j.biortech.2014.01.040>.
28. Kim S-S, Agblevor FA. Pyrolysis characteristics and kinetics of chicken litter. *Waste Manag.* 2007;27:135–40. <https://doi.org/10.1016/j.wasman.2006.01.012>.
29. Vamvuka D, Kakaras E, Kastanaki E, Grammelis P. Pyrolysis characteristics and kinetics of biomass residuals mixtures with lignite. *Fuel.* 2003;82:1949–60. [https://doi.org/10.1016/S0016-2361\(03\)00153-4](https://doi.org/10.1016/S0016-2361(03)00153-4).
30. Xue J, Ceylan S, Goldfarb JL. Synergism among biomass building blocks? Evolved gas and kinetics analysis of starch and cellulose co-pyrolysis. *Thermochim Acta.* 2015;618:36–47. <https://doi.org/10.1016/j.tca.2015.09.002>.

**Publisher's Note** Springer Nature remains neutral with regard to jurisdictional claims in published maps and institutional affiliations.